Hindawi
International Journal of Chemical Engineering
Volume 2022, Article ID 1821147, 12 pages
https://doi.org/10.1155/2022/1821147

Research Article

Comparative Study on Combustion and Flame Characteristics of Laminar Methane/Air and N-Butane/Air Flames in a Micro-Slot Burner

Soroush Sheykhbaglou and Seyed Mostafa Robati

School of Mechanical Aerospace and Maritime Engineering, Amirkabir University of Technology (Tehran Polytechnic), No. 350, Hafez Ave, Tehran, Iran

Correspondence should be addressed to Soroush Sheykhbaglou; soroush.sheykh@aut.ac.ir

Received 14 July 2022; Revised 12 October 2022; Accepted 26 October 2022; Published 15 November 2022

Academic Editor: Maksim Mezhericher

Combustion and flame characteristics of laminar methane/air and n-butane/air flames in a 3D-printed micro-slot burner is compared and reported in this study. The stability limit, flame appearance, and emission performance are investigated experimentally. In addition, past research on conventional burners is compared with the results of this study throughout the paper. The construction of this micro-slot burner was met by selective laser melting (SLM) process. Flame characteristics such as lift-off height, length, visible area, maximum width, and neck width are obtained using an image processing algorithm and are examined at different fuel and airflow rates. The results show that the blow-out limits of methane/air and n-butane/air flames are almost the same when compared at the same volume flow rates, although the methane/air flames are more stable than n-butane/air flames at the same thermal input powers. A region of interesting rope-like oscillatory flames (that has never been seen before in conventional burners) is observed in a small portion of a stable region for n-butane with a period ranging from 75.0 to 210.0 ms. It is also observed that the fuel type and fuel and airflow rates affect the flame shape and appearance and the flames formed by heavier fuel (n-butane) have longer length, lift-off height, maximum width, and visible area and lower neck width. Furthermore, methane/air flames exhibit lower values of CO and higher values of NO_x in the flue gas when compared to n-butane/air flames.

1. Introduction

Recently, as demand for microdevices such as microsatellites and micro-aerial vehicles has expanded, the need for a micropower source to power these systems has grown substantially. For extended durations of operation, these microsystems need high-density power sources. Typical hydrocarbon fuels have an energy density around 100 times that of the most modern batteries. Despite the heat losses associated with harvesting energy from fuel combustion, a microscale combustion system has been deemed a potential alternative to batteries [1–5]. Understanding the mechanics of laminar micro-flames is critical for developing such combustion devices because multiple micro-flames may be utilized concurrently to improve a heat source's overall heating effectiveness [6]. On the other hand, laminar flames have been widely studied for basic as well as practical reasons and may be used to evaluate numerical models [7–9]. Numerous benefits exist for the slot burner idea. This arrangement enables lengthy line-of-sight observations, reduced signal reabsorption for imaging, and reduced interference for off-axis scattering studies. Note out, slot burners provide exact lateral species profile measurements parallel to the long burner axis, that is, with the laser beam parallel to the long axis [10]. When developing a combustion device, it is essential to consider the form and size of the flame [11]. To get flame characteristics, threshold segmentation of photographs taken with a camera or high-speed recording is a simple and efficient way. Several similar papers on determining the shape of a flame using image processing can be found in [12–20]. Gao et al. [14] analyzed the flame length of buoyant turbulent slot flames. They developed an

approximate predictive correlation of flame length. They discovered that for the buoyancy-dominated and momentum-dominated flames, the flame length is proportional to $(Fr_m)^{1/3}$ and $(Fr_m)^0$, respectively. Zhou et al. [18] examined the flame height and lift-off height of rectangular source fuel jet fires. The buoyancy-momentum flame Froude number ranged from 0.38 to 3.06. It was observed that for a particular heat release rate when the aspect ratio increases, the flame height reduces. Zhen et al. [21] investigated the impact of substituting N_2 with CO_2 in coaxial-flow oxidizer of a double concentric burner on the combustion and emission of a diffusion flame. The fuel was methane and the oxidizer consisted of mixes of $N_2 - O_2$, $CO_2 - O_2$, and $N_2 - CO_2 - O_2$. They discovered that the flame lift-off height is linearly dependent on coaxial-flow velocity and the blow out of lifted flames occurs at a fixed tip height. The researchers also noticed that replacing N_2 with CO_2 significantly reduced the threshold coaxial-flow velocity for lift-off. In contrast, this threshold rises as the oxygen content in oxidizerincreases. In their investigation, they observed that prompt NO generation predominates and an increase in the velocity of $N_2 - O_2$ oxidizer, leads to a monotonic rise in NO_x, whereas the opposite is true for $CO_2 - O_2$. In these circumstances, CO always exhibits the opposite behavior of NO_x. Riahi et al. [22] investigated non-premixed oxygen and hydrogen enriched in a coaxial burner. This burner comprises of a jet of oxidizer (air and oxygen) encircling a central fuel mixture (natural gas and hydrogen). They discovered that hydrogen enrichment removes the lifted flame and creates a stable region. In addition, the oxygen enrichment reduces the creation of CO, but promotes the formation of NO_x. In microgravity, Zhang et al. [23] studied the properties of laminar jet coflowing diffusion flames. In microgravity, the experimental results demonstrated that laminar jet diffusion flames were significantly impacted by airflow velocities when there was no buoyancy. Increasing the coflowing air velocity increases the fuel-to-air mixing rate and draws the flame sheet closer to the nozzle. In addition, the maximum flame diameter and flame length decrease as air velocity increases. Tao et al. [17] studied the flame height and lift-off height of carbon dioxide-diluted propane turbulent jet diffusion flames at ambient temperature and pressure. They observed that the height of the flames lowers as the concentration of CO_2 increases. In addition, it was noted that the flame lift-off height increases with an increase in the concentration of CO_2 and is also proportional to fuel velocity (flow rate). Sady et al. [24] investigated the flame characteristics of premixed methane combustion using a ring attached-Bunsen burner. Flame temperature, flame height, and laminar flame speed were examined. As the ring temperature increases, the flame temperature and laminar flame speed rise while the flame length falls, according to the data. In addition, when the equivalency ratio approaches 1, flame temperature and laminar flame speed rise, but flame length demonstrates an opposite tendency. Zhou et al. [25] examined the stability and chemiluminescence characteristics of CH_4/O_2 lift-off inverse diffusion flames. They noticed that when the methane velocity grew, lift-off velocity fell; however, the blow out limit, flame height, and lift-off height increased. They also observed that lift-off velocity and lift-off height exhibited a linear relationship with methane velocity. The lift-off velocity is defined as the velocity of O_2 which led to flame lift-off from attachment. Anggarani et al. [26] compared jet diffusion flame characteristics and flame temperature of dimethyl ether (DME) and liquefied petroleum gas (LPG). DME produces a lower flame height than LPG, according to the data. The height of the flame generated by both fuels was unaffected by the diameter of the burner hole. The transitional regime in terms of Reynolds number differs greatly between DME and LPG, with DME reaching the transitional regime at a much lower Reynolds numbers. The flame temperature of DME is greater than that of LPG at the nozzle tip and in the dark zone. To the best of the author's knowledge, no comparative study on combustion and flame characteristics of laminar methane/air and n-butane/air flames in a 3D-printed micro-slot burner has been conducted. This investigation discovered an interesting region of rope-like oscillatory flames in the stability limits of n-butane/air flames that has never been seen before in conventional burners. In addition, past research on conventional burners is compared with the results of this study throughout the paper. As a consequence, this study is unique in analyzing and comparing combustion and flame characteristics of methane/air and n-butane/air flames in a micro slot burner. Flame charateristics including lift-off height, length, maximum width, neck width, and area are obtained using an image processing algorithm based on intermittency distribution method.

2. Experimental Setup

Figure 1(a) shows the schematic representation of the experimental setup and flow delivery system. Air and fuel including methane or n-butane are supplied from an air compressor and high-pressure cylinder, respectively and their pressures are then regulated using pressure reduction valves. The flow regulation of the air and fuel are met by AZBIL MPC0020 and KOBOLD DMS-5 mass flow controllers (±1% full scale accuracy), respectively. Flame images were captured using a Nikon V1 camera in its high-speed mode (400 fps) with a resolution of 640 × 240 and a Canon PowerShot G16 with a resolution of 4000 × 3000. The micro-slot burner which is depicted in more detail in Figure 1(b) is composed of three rectangular outlets, each with a dimension of 1 mm × 10 mm. The air and fuel flows are fed in the micro-slot burner in non-premixed mode and the fuel outlet is sandwiched between two airflow outlets. The construction of this burner which is made of SS 316L material was met by the selective laser melting (SLM) process with 1500 slices and 202 g powder in 6 hrs.

In order to study the emission performance of the burner, it was isolated from its environment by being inserted in ducts with two optical windows for recording images and videos. Concentrations of carbon monoxide (CO) and nitric oxides (NO_x) were recorded by a Testo-350XL flue gas analyzer. Flame characteristics including flames lift-off height, length, maximum width, neck width, and its visible area were obtained using an image processing technique called

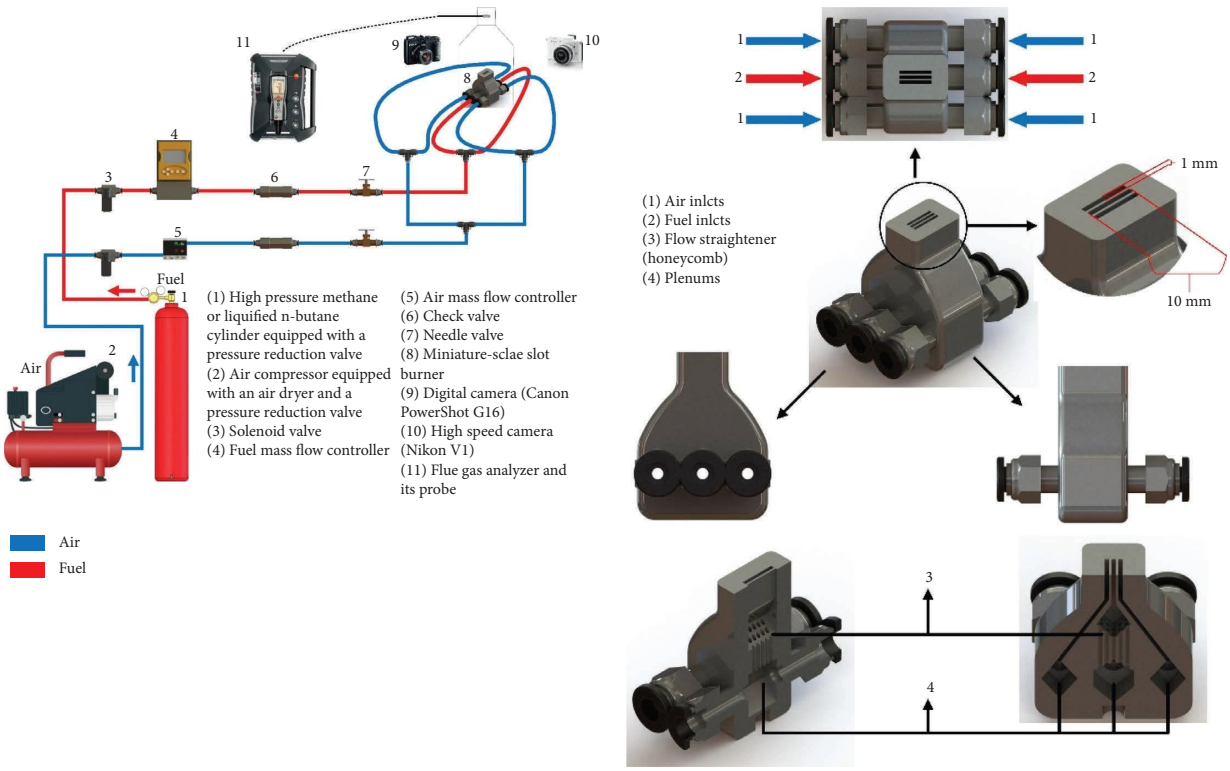

(a) (b)

Figure 1: (a) Experimental setup and flow delivery system; (b) micro-slot burner.

intermittency distribution in which the flame existence probability is used to calculate the flame characteristics. The steps of this procedure are shown in detail in Figure 2. 50 continuous flame images at predetermined values of fuel and air flow rates are preprocessed, and then a color threshold is applied to them and are binarized [27]. Finally, an intermittency threshold on 0.5 is applied to the average of binarized images and flame characteristics are obtained by converting image coordinates (pixels) to calibrated coordinates (mm) using the length of a known object in the image.

3. Results and Discussion

The stability limits of the burner, flame characteristics, and emission performance of non-premixed laminar methane/air and n-butane/air flames are investigated and compared in this section for three fuel flow rates and a variety of airflow rates within the stability limits.

3.1. Stability Limits. The approach used in [28] is employed to determine the stability limits of the burner for methane/air and n-butane/air flames. The procedure is as follows: (a) firstly, a predetermined value of fuel flow rate is fed to the micro-slot burner; (b) while keeping the igniter on, the air is fed in the burner gradually with an increment of 0.1 slpm to form a stable flame; (c) this increase of the air flow rate is continued until the flame extinguishes at the given fuel flow rate due to short residence time and insufficient time for mixing of fuel and air and their reaction (absence of flammable mixture) at the burner exit; (d) the airflow rate at which the flame extinguishes (blows out) is considered as the stability limit of the burner at the predetermined value of the fuel flow rate (Figure 3); (g) this procedure is repeated three time for each fuel flow rate and the average value is reported as the stability limits.

The stability limits of the burner are shown in Figure 4 for fuel flow rate varied from 0.100 to 0.500 slpm. Figure 4(a) shows these limits for methane and n-butane as the fuel, respectively, and Figure 4(b) compares these limits at the same input powers of methane and n-butane. It is observed that as the fuel flow rate increases, the stability limit shows an increasing trend (a similar trend is reported in [25]) and linear-dependent on the fuel flow rate. When the fuel flow rate is increased, more air is entrained into the fuel stream or more fuel diffuses into air and mixes with air due to recirculation zone induced at the same airflow rate [25], and more air is required to destabilize the flame. The following equation can be fitted to predict this dependence with $R^2 = 0.9937$ and 95% confidence bounds: $\dot{Q}_{air} = 2.067 \times \dot{Q}_{fuel} + 1.074$, in which $\dot{Q}_{fuel}$ is the fuel flow rate in slpm, and $\dot{Q}_{air}$ is the airflow rate at which the flame extinguishes (in slpm). It is also observed that the stability limits of both fuels of methane and n-butane are almost the same at given fuel flow rates; in other words, methane/air and n-butane/air flames extinguish at almost the same airflow rate where the fuel flow rate is fixed and the stability limits are independent of the fuel type and properties. On the other hand, when the input

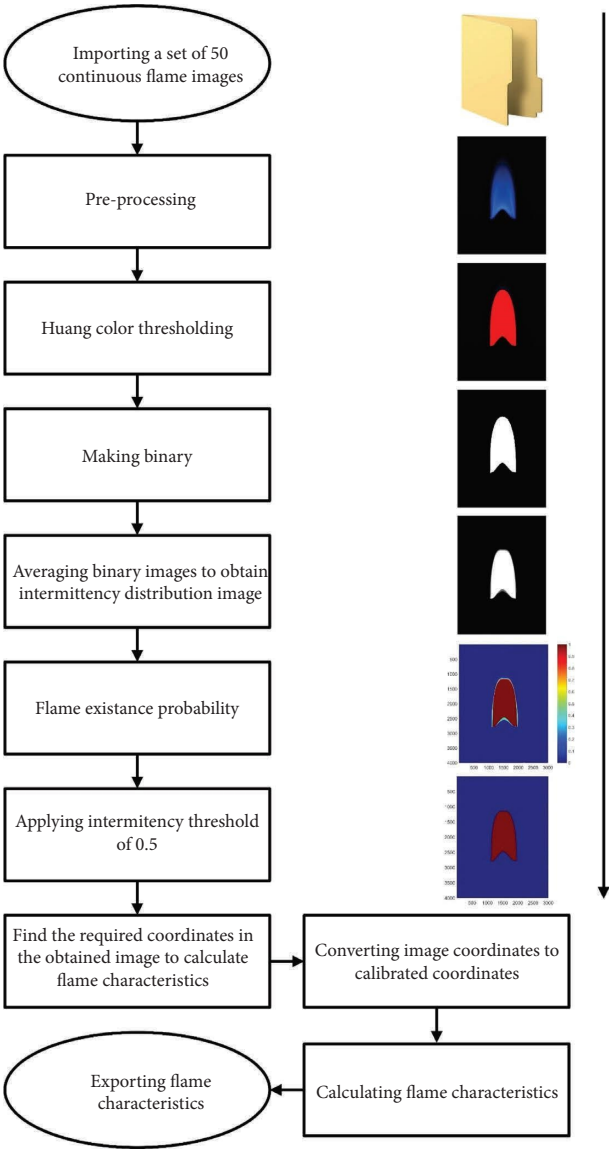

Figure 2: Procedure employed to calculate flame characteristics.

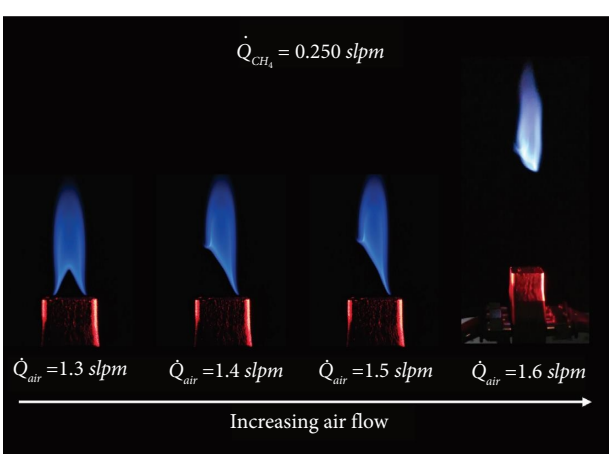

Figure 3: Flame blow out by increasing the airflow rate.

power is used to compare the stability limits of the abovementioned fuels, methane/air flames extinguish at higher airflow rates when the input power is fixed. When compared n-butane as fuel, using methane increases the stability limits by about 33, 38, and 43% at the input powers of 150, 200, and 250 W. In other words, methane/air flames can withstand a much higher airflow rate than n-butane/air flame at a given input power. Input powers are calculated based on the lower heating values (LHV) of the fuels. The same input power for both fuels results in a higher volumetric flow rate for methane (although methane has lower density than n-butane, but its LHV is higher). According to Figure 4(a), when the input power is fixed, methane/air flames have better stability limits than n-butane/air flames and extinguish at higher airflow rates (Figure 3) due to higher fuel flow rate and sufficient premixing with air after the burner exit plane.

A region of interesting rope-like oscillatory flames is observed in a small portion of a stable region for n-butane/air flames (Figure 5). As shown in Figure 6, the period of formed flames in this region ranges from 75.0 to 210.0 ms. It is observed that for fuel flow rates ranging from 0.040 to 0.060 slpm, the oscillatory flames occur at airflow rates equal to and larger than 1.0 slpm, and as the airflow rate increases (moving from lower limit to the upper limit, as depicted in Figure 5), the period on the oscillatory flames exhibits a decreasing trend; while for fuel flow rates greater than 0.060 slpm, these phenomena take place at airflow rates less than 1.0 slpm and period lengthens with an increment in the airflow rate; in other words, the flame oscillations are going to be suppressed. Figure 7 presents the behavior of flames formed at three sets of fuel and air flow rates in this region. These frames are extracted from high-speed video recordings with 400 frames per second (fps) using MATLAB. These oscillatory flames can be related to buoyancy-induced instability which results from interactions between the flame and vortices within and outside of the luminance flame. The outer toroidal vortices are caused by a Kelvin–Helmholtz instability generated by a buoyancy-induced shear layer encircling the flame surface [29, 30]. These rope-like reproducible oscillatory flames can be due to the acceleration of hot gases and periodic contact between the flame/vortices and the surrounding air. The flame bulge is created when the toroidal vortex below the bulge pushes the flame surface radially outward while the one above the bulge pulls the flame surface radially inward. As stated earlier for fuel flow rates greater than 0.060 slpm, the flame oscillation is suppressed by increasing the airflow rate. The reduction in Kelvin–Helmholtz and buoyancy-driven instabilities, as well as the shift in the initiation point of toroidal vortices (instability initiation point), may be the primary physical reason for this fascinating occurrence. In contrast, for fuel flow rates ranging from 0.040 to 0.060 slpm, increasing the airflow rate leads to a decrease in the period of these flames (an increase in the frequency) which can be attributed to significance of buoyant acceleration owing to a lower fuel flow rate and an increase in Kelvin–Helmholtz instability.

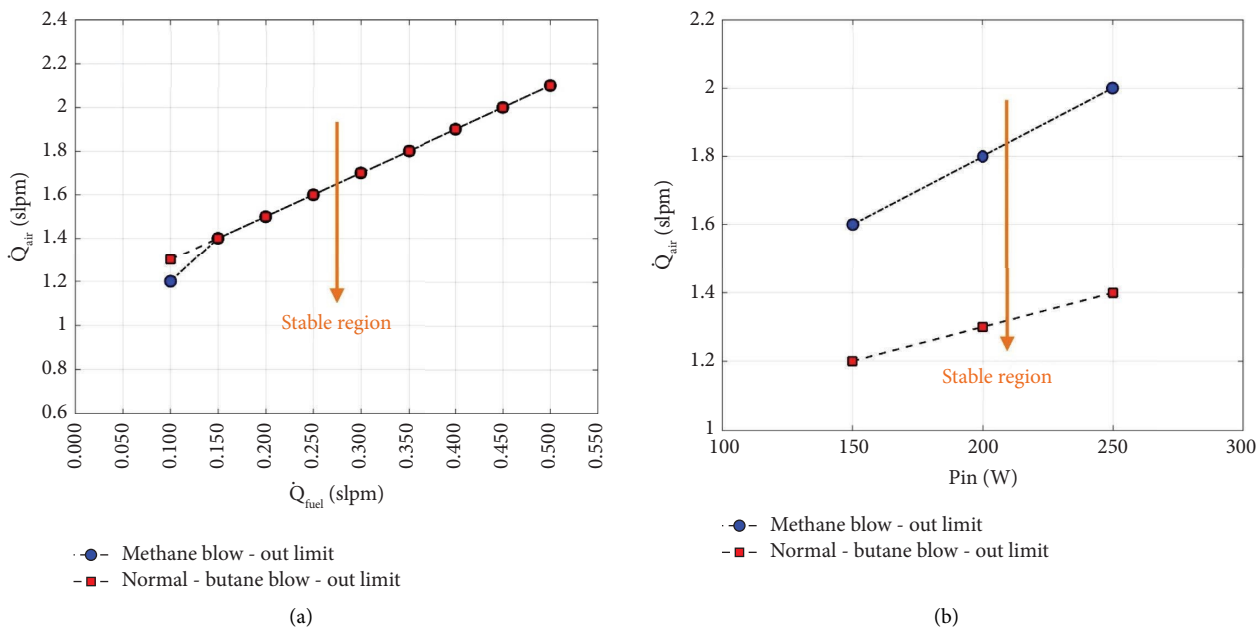

Figure 4: (a) Stability limits for methane and n-butane; (b) comparison of stability limits of methane and n-butane at the same input powers.

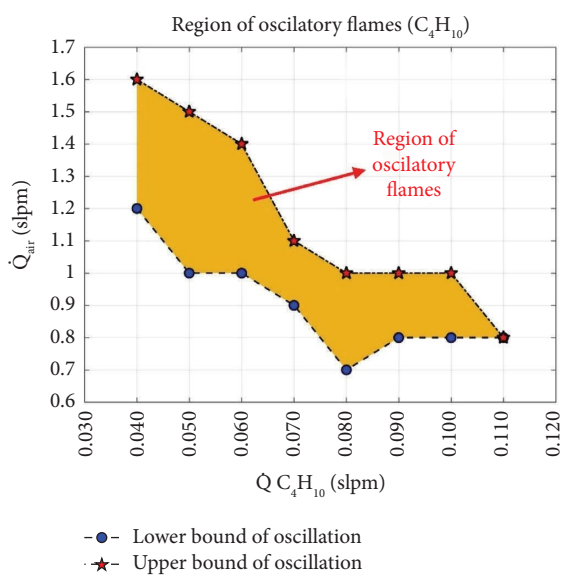

Figure 5: Region of oscillatory flames.

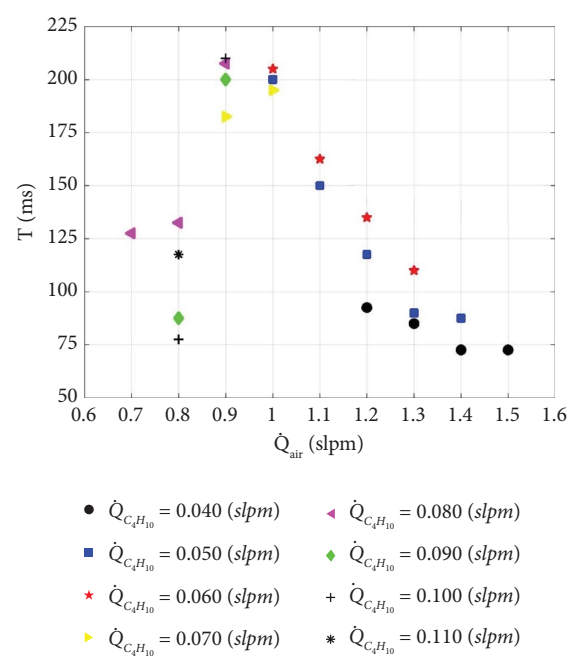

Figure 6: Periods of oscillatory flames.

3.2. Flame Characteristics. The evaluation of the flame structure and appearance aids in the comprehension of the physical processes that occur during combustion. These properties are influenced by geometrical configuration of the burner and air/fuel flow ratios. Figure 8 illustrates the effects of the airflow rate increase on the structure and appearance of methane/air (Figure 8(a)) and n-butane/air (Figure 8(b)) flames at the fuel flow rates of 0.200 and 0.150 slpm, respectively. With a constant fuel flow rate, increasing the airflow rate decreases the equivalence ratio. It is observed that the flames are composed of two yellow and blue parts in which the yellow one is an indication of diffusion combustion and soot formation and the blue one represents premixed combustion. According to [31], soot free length fraction (SFLF) is defined as the ratio of blue pat length to the length of the flame and the envelope of the blue zone is depicted in Figure 8. As the airflow rate increases, the length of the yellow part shortens and SFLF increases. For methane/air flames, the yellow region extinguishes by increasing the airflow rate; although this is not the case for n-butane/air flames and most of the flames formed by n-butane are comprised of the yellow part at low airflow rates. It is also observed that n-butane/air flames are more luminous than methane/air ones. Moreover, flame length exhibits a

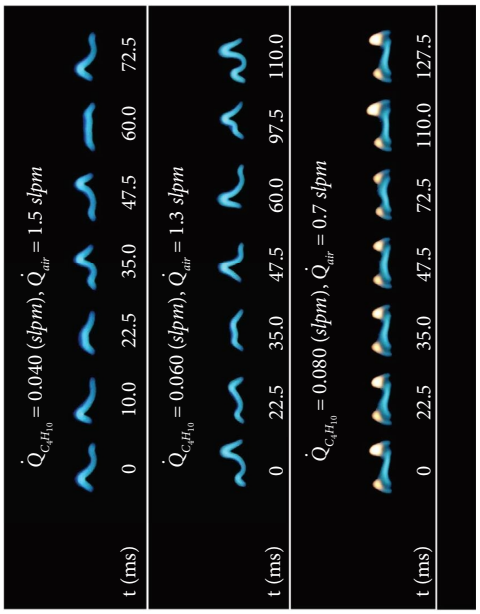

Figure 7: Examples of oscillatory flames at three operating conditions.

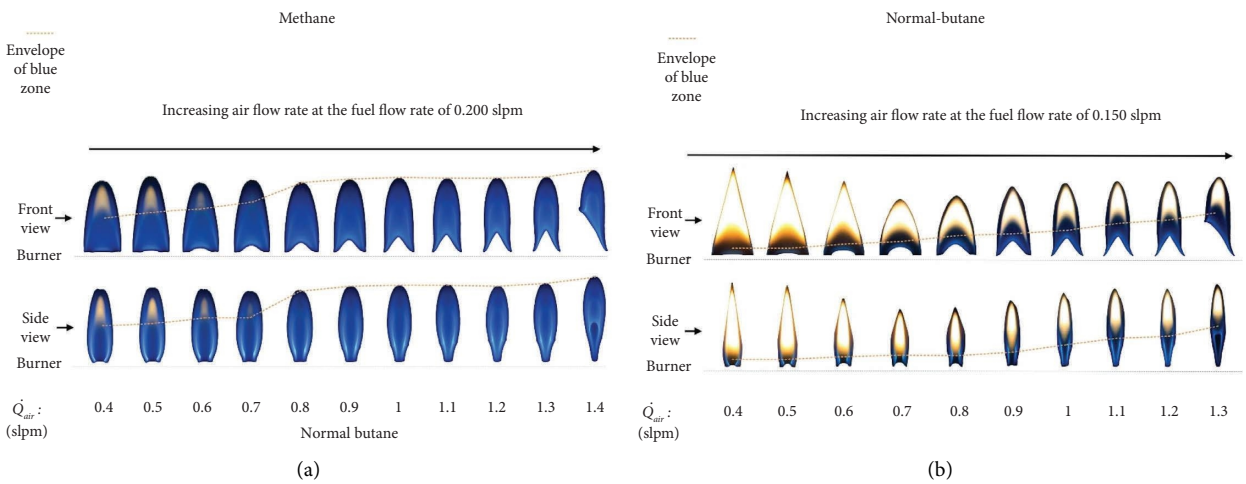

Figure 8: The effects of the airflow rate increase on the flame appearance and structure for (a) methane and (b) n-butane.

decreasing-increasing trend with an increment in the airflow rate, so the flame reaches a minimum length in some airflow rate (this is discussed in detail later). Figure 9 represents the effect of the fuel flow rate increase on the flame appearance where the airflow rate is fixed at 0.4 slpm. Increasing the fuel flow rate at a constant airflow rate rises the equivalence ratio. It is evident that as the fuel flow rate is increased from 0.050 to 0.250 slpm, SFLF decreases and the flame length increases. The SFLF decrease from 100% to about 50% for methane/air flames and about 50% to 10% for n-butane/air flames. It can be inferred that the fuel and air ratio and also fuel type affect the flame structure and appearance.

The size and form of the flame are the key factors in the design of a combustion system. In order to investigate and compare flame characteristics including flame lift-off height, length, maximum width, neck width, and the area which are defined in Figure 10, the intermittency distribution method which is depicted in Figure 2 is employed. The use of this method can be seen in other works too [12–14, 17–20, 27].

Figure 11 presents the flame lift-off variation with an increase in the airflow rate under three fuel flow rates. It is shown that as the airflow rate increases, flame lift-off increases monotonically and reveals almost linear dependence on the airflow rate where the fuel flow rate is fixed. Zhen et al. [21] reported a similar trend for a double concentric burner. They found that flame lift-off height reveals a linear increase with increasing coaxial-flow velocity (flow rate). Besides, increasing fuel flow rate rises the flame lift-off considering the airflow rate is constant. Zhou et al. [25] reported a similar trend. It is also shown that lift-off heights of n-butane/air flames are longer than methane/air flame under the same fuel and air flow rates; in other words,

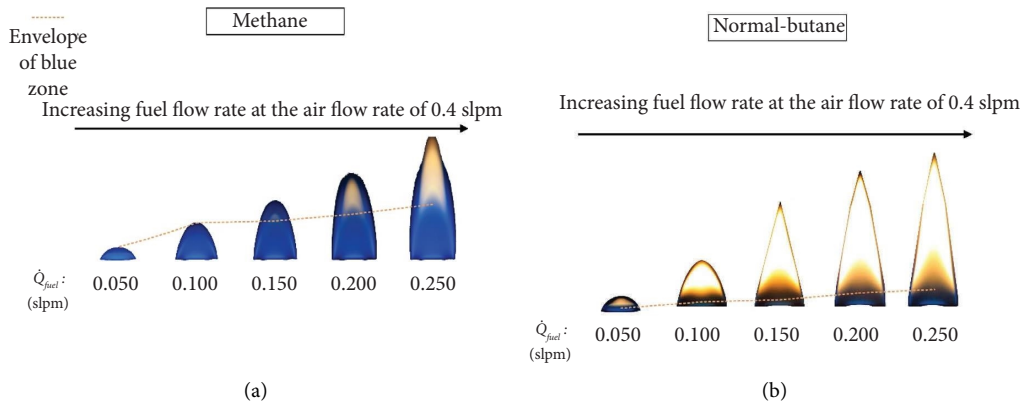

Figure 9: The effects of the fuel flow rate increase on the flame appearance and structure for (a) methane and (b) n-butane.

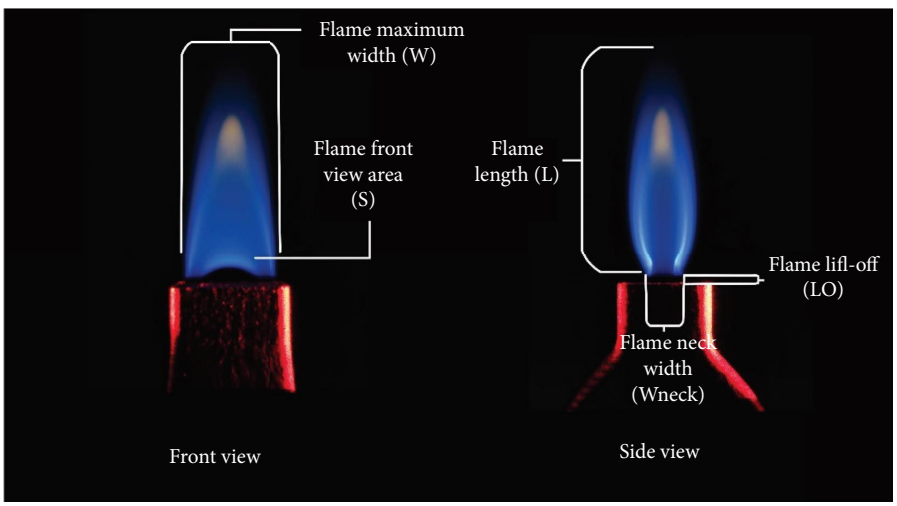

Figure 10: Definitions of flame characteristics.

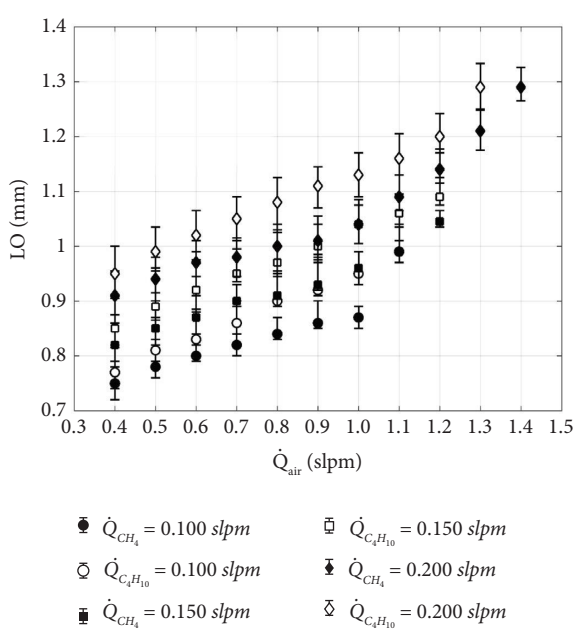

Figure 11: Variation of flame lift-off height with airflow rate for methane and n-butane.

n-butane/air flames form at a farther distance from the burner exit plane when compared to methane/air flames. This can be attributed to lower binary diffusion coefficient of n-butane/air in comparison to methane/air (lift-off is inversely proportional to diffusivity), which causes methane diffuse into air better than n-butane in the flame base which stabilizes the flame anchor position against the incoming airflow at lower distance from the burner exit plane [32, 33].

Figure 12 shows the effects of the airflow rate increase on the flame length for three different fuel flow rates. It is observed that the flame length reveals an almost decreasing-increasing dependence on the airflow rate increase and airflow rate at which the flame length reaches its minimum values, increases with an increase in the fuel flow rate. This can be attributed to an increase in the intensity of turbulence of air and combined effects of molecular transport and turbulent eddy mixing which enhances methane/air mixing and leads to a shorter flame length; although further increase in the airflow rate is not accompanied with an enhancement in methane/air mixing and lengthens the flame negligibly (Figure 8) and finally leads to blow out. A similar trend for flame length can be found in [14, 34–36] for increasing the fuel flow rate of a jet diffusion flame. Besides, increasing the

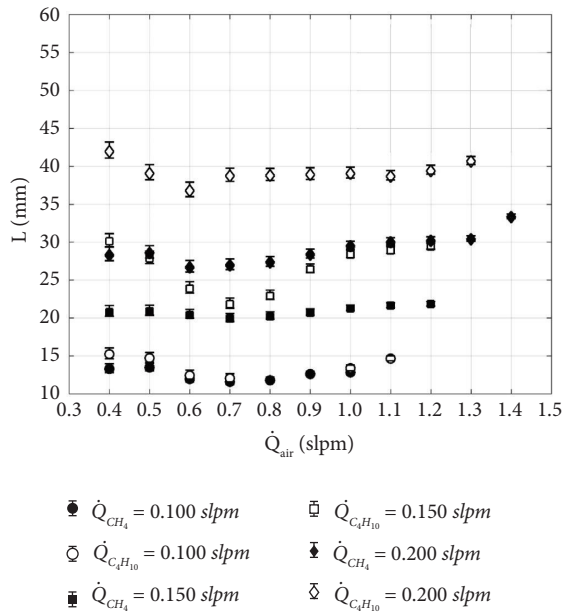

Figure 12: Variation of flame length with airflow rate for methane and n-butane.

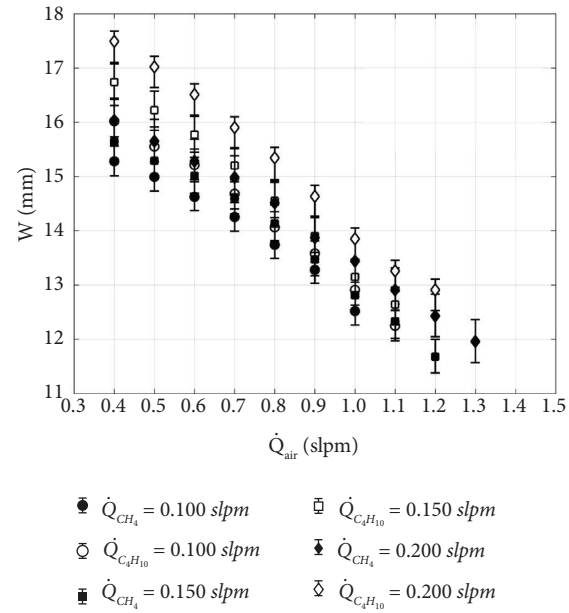

Figure 13: Variation of flame maximum width with the airflow rate for methane and n-butane.

fuel flow extends the flame length where the airflow rate is fixed because the fuel is not entrained and mixed by incoming air in an effective manner and mixes with air in a longer distance, so the flame elongates. It is also observed that n-butane/air flames are longer than methane/air flames at the same operating conditions. According to [34], the flame height of jet diffusion flames depends on the fuel type through its stoichiometry via an empirical correlation, and for a fixed volume flow rate of the fuel, flame height is proportional to S (molar stoichiometric air/fuel ratio). For methane and n-butane S is 9.52 and 30.94, respectively, so, n-butane jet flames reveal a higher flame height than methane jet flames, which is like the case for our study.

Figure 13 presents the effects of the airflow rate increase on the flame maximum width where the fuel flow rates are fixed. It is evident that the flame maximum width decreases almost linearly with an increase in the airflow rate for both fuels of methane and n-butane. Zhang et al. [23] also found that increasing coflowing air velocity decreases the maximum flame diameter. This can be attributed to a decrease in flow residence time as airflow rate increases, which reduces the amount of time fuel and air have to mix and react. It is also observed that as the fuel flow rate increases, the flame width increases, too. This can be related to the diffusion of more fuel into air with increasing the fuel flow rate at the same airflow rate. In addition, for the same fuel and air flow rates, n-butane/air flames are broader than methane/air flames, which can be explained by the greater molecular weight of n-butane compared to methane and the longer residence time for n-butane/air to coexist and mix in the direction perpendicular to the flow.

Figure 14 illustrates the effect of increasing the airflow rate on the width of the flame neck. This feature exhibits a similar tendency to the flame width as the airflow velocity

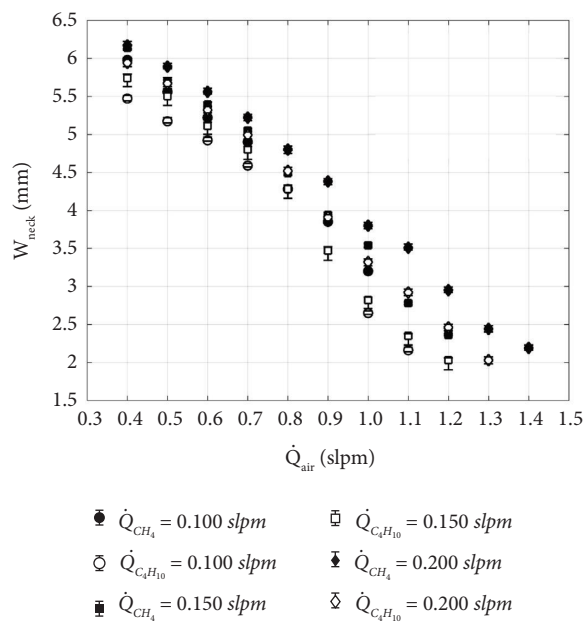

Figure 14: Variation of flame neck width with the airflow rate for methane and n-butane.

increases; however, methane/air flames have a larger neck than n-butane/air flames. Similar to Figure 13, the decrease in flame neck width with an increasing airflow rate can be attributed to the flow residence time. Figure 15 illustrates the impact of increasing the airflow rate on the flame area. As the airflow rate increases, the flame area drops monotonically in a linear pattern, which is due to a reduction in the flow residence time. On the other hand, n-butane/air flames have a bigger surface area than methane/air flames, and the area

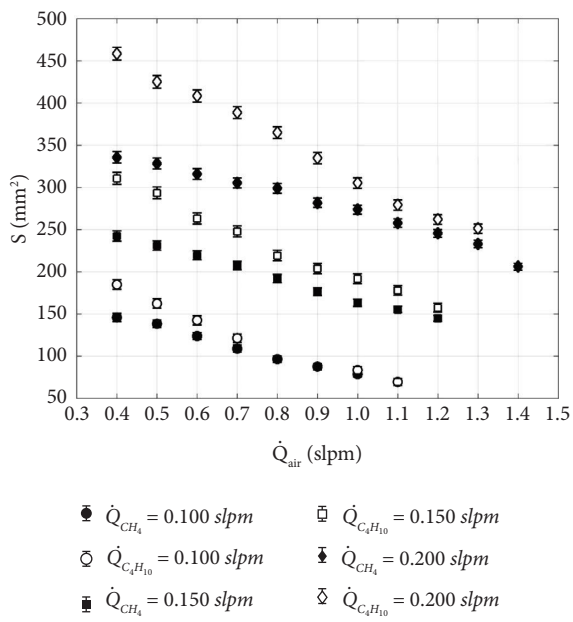

Figure 15: Variation of flame area with the airflow rate for methane and n-butane.

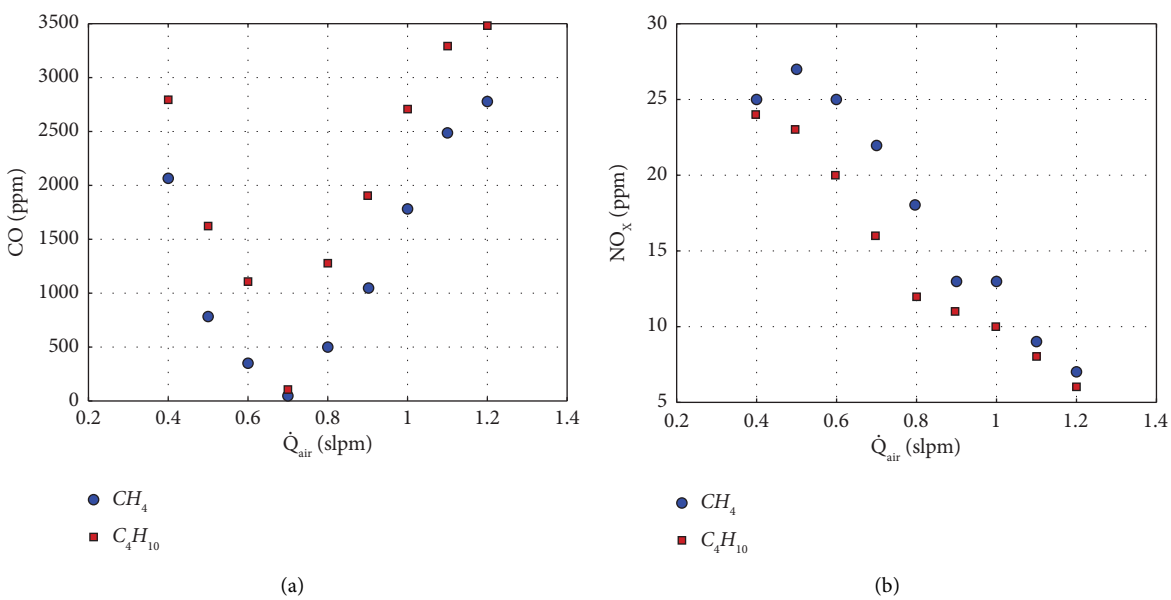

Figure 16: Variation of (a) CO and (b) NO_x concentration with airflow rate at the fuel flow rate of 0.150 slpm.

of n-butane/air flames reduces at a higher rate (bigger slope) compared to methane/air flames.

3.3. Emission Performance. Carbon monoxide (CO), unburned hydrocarbons (UHC), soot, nitric oxides (NO_x), sulfur oxides (SO_x), and metal oxides are the primary pollutants produced by combustion. They may be lessened to acceptable standards with a careful design. This section investigates and compares the CO and NO_x emissions from methane/air and n-butane/air flames under the fuel flow rate of 0.150 slpm and a range of airflow rates.

Low CO concentrations indicate that the combustion process is complete, since the majority of CO is oxidized to CO_2 and a large amount of heat is released [37]. CO oxidation occurs primarily through the following routes [34]:

(i) Wet route

$$CO + OH \longrightarrow CO_2 + H \quad (1)$$

In which OH radical is a determining species and is formed through the following reaction and can be inferred, that is, oxygen dependent:

$$H + O_2 \longrightarrow OH + O \quad (2)$$

(ii) Dry route

$$CO + O_2 \longrightarrow CO_2 + O \quad (3)$$

In this route, the availability of oxygen is of great importance in CO oxidation. Both routes are active at temperatures above 1100 K.

The variation of the CO concentration in the exhaust gas versus the airflow rate is shown in Figure 16(a) at the fuel flow rate of 0.150 slpm. It can be seen that CO exhibits a U-shaped dependence on the airflow rate increase. A similar trend can be found in [38]. At low airflow rates, the high values of CO can be attributed to O_2 availability which can terminate both routes of CO oxidation [39]. As the airflow rate is increased, the concentration of O_2 increases and can activate both routes and lead to a decrease in the CO level in the exhaust gas. At high airflow rates, the residence time of flow is short and fuel and air cannot mix properly which leads to incomplete combustion and high values of CO in the exhaust gas. It can be shown that n-butane/air flames result in higher values of CO at the exhaust gas compared to methane/air flames at the same operating conditions.

Figure 16(b) shows the effect of the airflow rate on NO_x emission in the exhaust gas. It is accepted that increasing residence time and temperature has an effect on NO formation through thermal mechanism, and this is the major mechanism in combustion processes over 1000 ℃ [40]. It is observed that NO_x concentration decreases monotonically as the airflow rate increases which can be due to a decrease in the flame temperature. Zhen et al. [21] reported a similar trend for $CO_2 - O_2$ coaxial flow, while a reverse trend for $N_2 - O_2$ flow. They also reported that the CO emission always vary in the opposite direction of NO_x, which is not the case for this study. Furthermore, NO_x levels in the exhaust gas are higher for n-butane/air flames which can be attributed to the higher flame length of n-butane/air flames. In n-butane/air flames, fuel and air mix at a longer distance (longer flame length) and heat releases over a longer distance when compared to methane/air flames which can reduce hot spots and consequently NO_x concentration.

4. Conclusion

In this study, combustion and flame characteristics of laminar methane/air and n-butane/air flames in a micro 3D-printed slot burner is investigated and compared. The major findings are as follows:

(i) The stability limits of methane/air and n-butane/air flames are linearly proportional to the fuel flow rate and rise monotonically as the fuel flow rate is increased. Both methane and n-butane flames blow out at almost the same airflow rate when compared to identical fuel flow rates; however, methane/air flames are more stable from an input power perspective than n-butane/air flames.

(ii) A region of interesting rope-like oscillatory flames is observed in a small portion of a stable region for n-butane with a period ranging from 75.0 to 210.0 ms.

(iii) The SFLF (soot free length fraction) increases by increasing the airflow rate where the fuel flow rate is fixed; while this property decreases from 100% to about 50% for methane/air flames and about 50% to 10% for n-butane/air flames by increasing the fuel flow rate from 0.050 to 0.250 slpm at the airflow rate of 0.4 slpm. It can be inferred that the fuel and air ratio and also the fuel type affect the flame structure and appearance.

(iv) An image processing algorithm based on the intermittency distribution method was utilized to calculate the flame characteristics including flame lift-off height, length, maximum width, neck width, and the area. It is found that n-butane flames have greater length, lift-off height, maximum width, and visible area and narrower neck width compared to methane/air flames.

(v) CO emission in the exhaust gas shows a U-shaped dependence on the airflow rate increase where the fuel flow rate is fixed; while NO_x decreases linearly with an increase in the airflow rate. Methane/air flames exhibit lower values of CO and higher values of NO_x in the flue gas when compared to n-butane/air flames.

Data Availability

All data that support the findings of this study are included within the article.

Additional Points

(i) Combustion and flame characteristics of laminar methane/air and n-butane/air flames in a micro 3D-printed slot burner is investigated and compared. (ii) The flame stability shows a linear dependence on the fuel flow rate for both types of fuels. (iii) An image processing algorithm based on intermittency distribution method is utilized to obtain flame characteristics. (iv) A region of interesting rope-like oscillatory flames is observed in a small portion of a stable region for n-butane with period a ranging from 75.0 to 210.0 ms. (v) Methane/air flames exhibit lower values of CO and higher values of NO_x in the flue gas when compared to n-butane/air flames. (vi) In comparison to methane/air flames, n-butane flames have a greater length, lift-off height, maximum width, and visible area and a narrower neck width.

Conflicts of Interest

The authors declare that they have no conflicts of interest.

References

[1] K. Maruta, "Micro and mesoscale combustion," *Proceedings of the Combustion Institute*, vol. 33, no. 1, pp. 125–150, 2011.

[2] W. Wang, Z. Zhao, N. Kuang, H. Chen, J. Liu, and Z. Zuo, "Experimental study and optimization of a combustion-based micro thermoelectric generator," *Applied Thermal Engineering*, vol. 181, Article ID 115431, 2020.

[3] H. Li, Y. Chen, Y. Yan, C. Hu, H. Fan, and S. Feng, "Numerical study on heat transfer enhanced in a microcombustor with staggered cylindrical array for micro-thermophotovoltaic system," *Journal of Energy Resources Technology*, vol. 140, no. 11, 2018.

[4] Y. Yan, Y. Liu, H. Li et al., "Effect of cavity coupling factors of opposed counter-flow microcombustor on the methane-fueled catalytic combustion characteristics," *Journal of Energy Resources Technology*, vol. 141, no. 2, 2018.

[5] S. Sheykhbaglou and S. M. Robati, "Development of a small power generation system with a miniature-scale swirl burner, controlled heat transfer, and thermoelectric generators," *Engineering Research Express*, vol. 4, no. 2, Article ID 025006, 2022.

[6] K. Kuwana, S. Kato, A. Kosugi, T. Hirasawa, and Y. Nakamura, "Experimental and theoretical study on the interaction between two identical micro-slot diffusion flames: burner pitch effects," *Combustion and Flame*, vol. 165, pp. 346–353, 2016.

[7] J. Min, F. Baillot, H. Guo, E. Domingues, M. Talbaut, and B. Patte-Rouland, "Impact of CO_2, N_2 or Ar diluted in air on the length and lifting behavior of a laminar diffusion flame," *Proceedings of the Combustion Institute*, vol. 33, no. 1, pp. 1071–1078, 2011.

[8] P. B. Sunderland, J. E. Haylett, D. L. Urban, and V. Nayagam, "Lengths of laminar jet diffusion flames under elevated gravity," *Combustion and Flame*, vol. 152, no. 1-2, pp. 60–68, 2008.

[9] Z. Wang, P. B. Sunderland, and R. L. Axelbaum, "Dilution effects on laminar jet diffusion flame lengths," *Proceedings of the Combustion Institute*, vol. 37, no. 2, pp. 1547–1553, 2019.

[10] M. F. Campbell, G. A. Bohlin, P. E. Schrader et al., "Design and characterization of a linear Hencken-type burner," *Review of Scientific Instruments*, vol. 87, no. 11, Article ID 115114, 2016.

[11] Z. Xi, Z. Fu, X. Hu, S. W. Sabir, and Y. Jiang, "An investigation on flame shape and size for a high-pressure turbulent non-premixed swirl combustion," *Energies*, vol. 11, no. 4, p. 930, 2018.

[12] L. Huang, C. Liu, T. Deng, H. Jiang, and P. Wu, "Experimental investigation on the influence of central airflow on swirl combustion stability and flame shape," *Journal of Thermal Analysis and Calorimetry*, vol. 144, no. 2, pp. 503–514, 2021.

[13] S. Zhang, X. Cheng, K. Zhu, Y. Yao, L. Shi, and H. Zhang, "Experimental study on curved flame characteristics under longitudinal ventilation in a subway tunnel," *Applied Thermal Engineering*, vol. 114, pp. 733–743, 2017.

[14] W. Gao, N. Liu, Y. Jiao et al., "Flame length of non-buoyant turbulent slot flame," *Proceedings of the Combustion Institute*, vol. 37, no. 3, pp. 3843–3850, 2019.

[15] X. Sun, L. Hu, F. Ren, and K. Hu, "Flame height and temperature profile of window ejected thermal plume from compartment fire without facade wall," *International Journal of Thermal Sciences*, vol. 127, pp. 53–60, 2018.

[16] K. Xie, Y. Cui, C. Wang et al., "Study on threshold selection method of continuous flame images of spray combustion in the low-pressure chamber," *Case Studies in Thermal Engineering*, vol. 26, Article ID 101195, 2021.

[17] C. Tao, B. Liu, Y. Dou, Y. Qian, Y. Zhang, and S. Meng, "The experimental study of flame height and lift-off height of propane diffusion flames diluted by carbon dioxide," *Fuel*, vol. 290, Article ID 119958, 2021.

[18] Z. Zhou, G. Chen, C. Zhou, K. Hu, and Q. Zhang, "Experimental study on determination of flame height and lift-off distance of rectangular source fuel jet fires," *Applied Thermal Engineering*, vol. 152, pp. 430–436, 2019.

[19] T. B. Maynard and J. W. Butta, "A physical model for flame height intermittency," *Fire Technology*, vol. 54, no. 1, pp. 135–161, 2018.

[20] S. Sheykhbaglou and S. M. Robati, "Effects of coaxial airflow swirl number on combustion and flame characteristics of methane/air and n-butane/air flames in a miniature-scale swirl burner," *Engineering Research Express*, vol. 4, no. 2, Article ID 025045, 2022.

[21] H. Zhen, Z. Wei, and Z. Chen, "Effect of N_2 replacement by CO_2 in coaxial-flow on the combustion and emission of a diffusion flame," *Energies*, vol. 11, no. 5, p. 1032, 2018.

[22] Z. Riahi, M. A. Mergheni, J.-C. Sautet, and S. Ben Nasrallah, "Experimental study of natural gas flame enriched by hydrogen and oxygen in a coaxial burner," *Applied Thermal Engineering*, vol. 108, pp. 287–295, 2016.

[23] D. Zhang, J. Fang, J.-F Guan et al., "Laminar jet methane/air diffusion flame shapes and radiation of low air velocity coflow in microgravity," *Fuel*, vol. 130, pp. 25–33, 2014.

[24] I. E. Sady, A. S. Widodo, F. G. Utami Dewi, and Trismawati, "Flame characteristics analysis of a methane gas' premixed combustion on a ring attached-bunsen burner using ansys fluent," *Journal of Physics: Conference Series*, vol. 2193, no. 1, Article ID 012006, 2022.

[25] Y. Zhou, F. Xie, M. Yao, X. Song, Y. Bai, and G. Yu, "Investigation on stability and chemiluminescence characterization for liftoff inverse diffusion flames," *Combustion Science and Technology*, vol. 194, no. 12, pp. 2461–2479, 2022.

[26] R. Anggarani, C. S. Wibowo, Maymuchar, and I. M. K. Dhiputra, "Comparison of jet diffusion flame characteristics and flame temperature of dimethyl ether (DME) and liquefied petroleum gas (LPG)," *IOP Conference Series: Materials Science and Engineering*, vol. 694, no. 1, Article ID 012019, 2019.

[27] S. Sheykhbaglou and S. Karami, "Comparative study on threshold selection for measuring characteristics of turbulent swirling flames in a miniature-scale swirl burner," *Signal, Image and Video Processing*, 2022.

[28] R. Alsulami and B. Windom, "Liquid jet fuel property impacts on combustion performance," *Journal of Propulsion and Power*, vol. 37, no. 2, pp. 276–282, 2021.

[29] G. Darabkhani and Y. Zhang, "Suppression dynamics of a laminar oscillating diffusion flame with co-flow air," *Lecture Notes in Engineering and Computer Science*, vol. 2, 2010.

[30] A. Lingens, M. Reeker, and M. Schreiber, "Instability of buoyant diffusion flames," *Experiments in Fluids*, vol. 20, no. 4, pp. 241–248, 1996.

[31] V. Patel and R. Shah, "Experimental investigation on flame appearance and emission characteristics of LPG inverse diffusion flame with swirl," *Applied Thermal Engineering*, vol. 137, pp. 377–385, 2018.

[32] S. R. Turns, *An Introduction to Combustion: Concepts and Applications*, McGraw-Hill, New York, NY, USA, 2012.

[33] R. W. Elliott and H. Watts, "Diffusion of some hydrocarbons in air: a regularity in the diffusion coefficients of a homologous series," *Canadian Journal of Chemistry*, vol. 50, no. 1, pp. 31–34, 1972.

[34] S. McAllister, J. Y. Chen, and A. C. Fernandez-Pello, *Fundamentals of Combustion Processes*, Springer, New York, NY, USA, 2011.
[35] I. Glassman, R. A. Yetter, and N. G. Glumac, *Combustion*, Academic Press, Cambridge, MA, USA, 2014.
[36] Y. Kang, T. Lu, X. Lu et al., "On predicting the length, width, and volume of the jet diffusion flame," *Applied Thermal Engineering*, vol. 94, pp. 799–812, 2016.
[37] Z. Xi, Z. Fu, X. Hu, S. W. Sabir, and Y. Jiang, "An experimental investigation on the NO and CO emission characteristics of a swirl convergent-divergent nozzle at elevated pressure," *Energies*, vol. 11, no. 6, p. 1410, 2018.
[38] R. Jarpala, N. V. S. Aditya Burle, M. Voleti, and R. Sadanandan, "Effect of swirl on the flame dynamics and pollutant emissions in an ultra-lean non-premixed model gas turbine burner," *Combustion Science and Technology*, vol. 189, no. 10, pp. 1832–1848, 2017.
[39] H. Zhen, B. Du, X. Liu, Z. Liu, and Z. Wei, "Experimental investigation on the heat flux distribution and pollutant emissions of slot LPG/air premixed impinging flame array," *Energies*, vol. 14, no. 19, p. 6255, 2021.
[40] C. E. Baukal Jr., *The John Zink Hamworthy Combustion Handbook: Volume 1-Fundamentals*, CRC Press, Boca Raton, FL, USA, 2013.